HHS Public Access

Author manuscript

Fetal Diagn Ther. Author manuscript; available in PMC 2019 January 01.

Published in final edited form as:

Fetal Diagn Ther. 2018 ; 43(4): 304–316. doi:10.1159/000468929.

Prenatal diagnosis of dextrocardia with complex congenital heart disease using Fetal Intelligent Navigation Echocardiography (FINE) and a literature review

Lami Yeo, MD[1,2,3], **Suchaya Luewan, MD**[1,4], **Dor Markush, MD**[5], **Navleen Gill, MD**[1,2,3], and **Roberto Romero, MD, D.Med.Sci.**[1,6,7,8]

[1]Perinatology Research Branch, Program for Perinatal Research and Obstetrics, Division of Intramural Research, Eunice Kennedy Shriver National Institute of Child Health and Human Development, NIH, Bethesda, MD and Detroit, MI, USA [2]Detroit Medical Center, Hutzel Women's Hospital, Detroit, MI, USA [3]Department of Obstetrics and Gynecology, Wayne State University School of Medicine, Detroit, MI, USA [4]Department of Obstetrics and Gynecology, Chiang Mai University, Chiang Mai, Thailand [5]Department of Pediatrics, Wayne State University School of Medicine, Children's Hospital of Michigan, Detroit, MI, USA [6]Department of Obstetrics and Gynecology, University of Michigan, Ann Arbor, MI, USA [7]Department of Epidemiology and Biostatistics, Michigan State University, East Lansing, MI, USA [8]Center for Molecular Medicine and Genetics, Wayne State University, Detroit, MI, USA

Abstract

Fetal dextrocardia is a type of cardiac malposition where the major axis from base to apex points to the right side. This condition is usually associated with a wide spectrum of complex cardiac defects. As a result, dextrocardia is conceptually difficult to understand and diagnose on prenatal ultrasound. The advantage of four-dimensional sonography with spatiotemporal image correlation (STIC) is that this modality can facilitate fetal cardiac examination. A novel method known as Fetal Intelligent Navigation Echocardiography (FINE) allows automatic generation of nine standard fetal echocardiography views in normal hearts by applying intelligent navigation technology to STIC volume datasets. In fetuses with congenital heart disease, FINE is also able to demonstrate abnormal cardiac anatomy and relationships when there is normal cardiac axis and position. However, this technology has never been applied to cases of cardiac malposition. We report herein for the first time, a case of fetal dextrocardia and situs solitus with complex congenital heart disease in which the FINE method was invaluable in diagnosing multiple abnormalities and defining complex anatomic relationships. We also review the literature on prenatal sonographic diagnosis of dextrocardia (with an emphasis on situs solitus), as well as tricuspid atresia with its associated cardiac features.

Address correspondence to: Lami Yeo, MD and Roberto Romero, MD, D. Med. Sci., Perinatology Research Branch, NICHD, NIH, DHHS, Hutzel Women's Hospital, 3990 John R, 4 Brush, Detroit, MI 48201, USA, Telephone (313) 993-2700, Fax: (313) 993-2694, lyeo@med.wayne.edu and prbchiefstaff@med.wayne.edu.

Keywords

4D ultrasound; cardiac malposition; fetal heart; prenatal diagnosis; spatiotemporal image correlation; STIC; transposition of great vessels; tricuspid atresia; ultrasound; VIS-Assistance®

Introduction

Assessment of fetal cardiac axis and position is routinely performed on prenatal ultrasound examinations. Primary dextrocardia is a type of cardiac malposition where the major axis of the heart (from base to apex along the interventricular septum) points to the right, and is due to an intrinsic developmental abnormality [1–5]. This should be distinguished from secondary dextrocardia (or dextroposition), in which the heart is shifted into the right chest due to pathology related to the diaphragm, lung, pleura, or other adjoining tissues, while the cardiac apex points to the left [2, 4–6]. The term *dextrocardia*, however, describes only the position of the cardiac axis, and does not convey information about chamber organization and cardiac anatomy [2,3,4,7–10].

The incidence of fetal primary dextrocardia has been reported to be 0.22-0.83% in tertiary fetal cardiology units [2,4,5]. Since fetal dextrocardia is usually associated with a wide spectrum of cardiac defects that are often complex [2,4,5,11], this condition is conceptually difficult to understand and diagnose [3,7,11]. Therefore, using ultrasound, a careful segmental analysis of cardiac anatomy is important to analyse and define the anatomical relationships [8]. Yet, this task can be very difficult even for experienced sonologists, making prenatal diagnosis challenging.

There is a growing body of evidence suggesting that four-dimensional (4D) sonography with spatiotemporal image correlation (STIC) can facilitate examination of the fetal heart [12–26]. STIC technology allows acquisition of a fetal cardiac volume data set and displays a cine loop of a complete single cardiac cycle in motion [13–15,27,28]. Such volume datasets allow sonologists to extract and display cardiac planes in any orientation. Therefore, 4D sonography with STIC has been proposed in both cardiac screening and the prenatal diagnosis of congenital heart disease [29–35], since it improves the identification of complex intracardiac relationships [12]. Yet, the manipulation and analysis of STIC volume datasets is operator dependent and can be an arduous task, especially when the fetal heart is abnormal.

Recently, a novel method known as Fetal Intelligent Navigation Echocardiography (FINE) was developed, which automatically generates and displays nine standard fetal echocardiography views in normal hearts by applying “intelligent navigation” technology to STIC volume datasets [12,36–39]. FINE can simplify examination of the fetal heart and reduce operator dependency [36]. Moreover, in cases of congenital heart disease, FINE is able to demonstrate abnormal fetal cardiac anatomy in multiple echocardiography views [36]. However, such method has never been applied thus far to cases of fetal cardiac malposition, such as dextrocardia.

We report herein for the first time, a case of situs solitus and dextrocardia with complex congenital heart disease (tricuspid atresia type II, D-transposition of the great vessels, hypoplastic right ventricle, coarctation of the aorta, ventricular septal defect, and atrial septal defect) that was diagnosed in the third trimester using FINE. Such method was invaluable in demonstrating the specific abnormalities and defining the complex anatomic relationships, which had been very difficult to do on real-time echocardiography.

Clinical Case

A 28-year-old, healthy multiparous (G5, P2022) patient was referred to our research ultrasound unit at 35 weeks of gestation for a complex congenital heart defect. We examined the patient at the Detroit Medical Center/Wayne State University, and the Perinatology Research Branch of NICHD, NIH, DHHS. She was enrolled in a research protocol approved by the Institutional Review Board of NICHD, NIH, and by the Human Investigation Committee of Wayne State University. The patient provided written informed consent for the use of sonographic images for research purposes. It is noteworthy that since its original invention [36], the FINE method has been integrated into a commercially available ultrasound platform (UGEO WS80A; Samsung Healthcare, Seoul, Korea) and is known as *5D Heart* technology.

Her past medical history was significant for a bicornuate uterus with the fetus located in the right horn, vaginal septum, and two prior cesarean deliveries. The patient's pre-pregnancy body mass index was 40.5 kg/m^2, which is classified as extremely obese [40–41].

The patient had presented late into prenatal care (27 gestational weeks) to another physician, and was transferred to our Maternal-Fetal Medicine clinic at 29 weeks due to the fetal cardiac diagnosis. Ultrasound examinations had been performed by both the clinical ultrasound unit and pediatric cardiology, in which dextrocardia was diagnosed. However, based upon real-time fetal echocardiography examinations, it was not clear as to whether there was a hypoplastic right or left heart, situs solitus or situs ambiguous, atrio-ventricular discordance (ventricular inversion), congenitally corrected transposition of the great vessels, or anomalous pulmonary venous return. Amniocentesis testing had been declined by the patient. However, non-invasive prenatal screening showed a male fetus with a low risk for trisomy 21, 18, 13, monosomy X, and triploidy.

At 35 weeks of gestation, the patient underwent a fetal echocardiographic examination by pediatric cardiology. Such study was noted to be technically difficult and suboptimal due to advanced gestational age and significantly decreased amniotic fluid volume. Therefore, the imaging planes were suboptimally obtained. The following was noted on the exam: 1) situs ambiguous with dextrocardia; 2) ventricular inversion with congenitally corrected transposition of the great vessels; 3) common atrium; 4) while the superior vena cava was identified returning to the atrial mass, the inferior vena cava was not identified, and an interrupted inferior vena cava with azygos vein continuation could not be excluded; 5) pulmonary veins were not identified; 6) severely hypoplastic tricuspid valve (vs. atresia) and enlarged mitral valve with dysplastic leaflets; 7) hypoplastic right ventricle and dilated left ventricle; 8) intact ventricular septum; 9) moderately dilated pulmonary valve annulus and

aortic valve atresia; and 10) ductal arch appeared widely patent; however, the aortic arch was not well visualized.

Examination of the fetal heart using FINE

On the same day but several hours later, the patient came to our research ultrasound unit and a 4D sonographic examination with STIC was performed. As soon as she arrived, the patient imposed specific time constraints and therefore, the fetal cardiac examination was performed expeditiously and was limited in nature. We noted fetal growth restriction (estimated fetal weight $<5^{th}$ percentile) and a decreased amniotic fluid index of 7.9 cm. Yet, despite the advanced gestational age, amniotic fluid volume, and extreme obesity, we immediately recognized that conditions were appropriate to acquire STIC volume datasets [27,28]. For example, the fetal spine was located at the 6-o'clock position, there was minimal shadowing of the four-chamber view and upper mediastinum, as well as absent fetal breathing and gross movements [28]. Therefore, within 6 minutes of beginning the ultrasound examination, multiple STIC volume datasets of the fetal heart were acquired from the apical four-chamber view by transverse sweeps through the fetal chest. The patient was asked to momentarily suspend breathing during STIC acquisition. The acquisition time was 10 seconds, while the acquisition angle was 40 degrees.

A single STIC volume dataset considered to be of highest quality was chosen for analysis by FINE. Next, using the Anatomic Box® feature, seven anatomical structures of the fetal heart were marked on the screen to generate an internal geometrical model of such heart [36–38]. The structures in sequential order are: 1) cross-section of the aorta at the level of the stomach; 2) cross-section of the aorta at the level of the four-chamber view; 3) crux; 4) right atrial wall; 5) pulmonary valve; 6) cross-section of the superior vena cava; and 7) transverse aortic arch. Once marking is completed, FINE allows nine standard fetal echocardiography views to be automatically generated and displayed: 1) four chamber; 2) five chamber; 3) left ventricular outflow tract; 4) short-axis view of great vessels/right ventricular outflow tract; 5) three-vessels and trachea (3VT); 6) abdomen/stomach; 7) ductal arch; 8) aortic arch; and 9) superior and inferior venae cavae [12,36,38].

The nine fetal echocardiography views are displayed simultaneously in a single template as nine *diagnostic planes* (Figure 1 and Videoclip S1; for all online supplementary material, see www.karger.com/doi/10.1159/000468929). As part of the FINE method, the operator-independent Virtual Intelligent Sonographer Assistance (VIS-Assistance®) tool can also be activated for each of the nine cardiac diagnostic planes. This tool essentially functions as a virtual sonologist which "scans" the STIC volume in a targeted way (as a videoclip) to yield additional information within a specified territory of the diagnostic plane [12,36–38]. Since VIS-Assistance® navigates and explores the surrounding structures in each of the nine diagnostic planes, it accomplishes the following: 1) improves the success of obtaining the fetal echocardiography view of interest; 2) provides additional information that is not evident in the diagnostic plane; 3) reduces the false-positive rate; and 4) improves the quality of the fetal cardiac examination [12,36–38]. Indeed, we have found VIS-Assistance® to be particularly informative and valuable in cases of congenital heart disease [36,39]. It is noteworthy that in three VIS-Assistance® views, the following structures are also

automatically shown in the videoclip: 1) 3VT: three-vessel view and transverse aortic arch; 2) abdomen/stomach: stomach and four-chamber view (to determine situs); and 3) four-chamber: atrial septum (both septum primum and septum secundum) and pulmonary veins [12,36,38].

An additional novel feature of FINE is that automatic labeling occurs of the nine echocardiography views (i.e. diagnostic planes), anatomical structures, left and right sides of the fetus, and cranial and caudal ends [36,37]. The purpose of such labeling is to assist readers of images in recognizing anatomical structures, and also to allow the images generated by FINE for a particular case to be compared with what is considered normal [37]. Automatic labeling is an optional feature and may be activated or turned off.

After applying the FINE (or 5D Heart) method to the STIC volume dataset, we noted that all nine echocardiography views were abnormal (Figure 1 and Videoclip S1). The 3VT diagnostic plane/VIS-Assistance® shows the well-developed leftward pulmonary artery arising from the dilated morphologic left ventricle, while a hypoplastic aorta is rightward and anterior to the pulmonary artery, and arises from the hypoplastic morphologic right ventricle (i.e. D-transposition of the great vessels). A few points are noteworthy. The degree of hypoplasia of the aorta is related to the size of the right ventricle, as well as the size of the ventricular septal defect (VSD). In the 3VT view of a normal heart, the transverse aortic arch/isthmus merge with the pulmonary trunk/ductus arteriosus into the descending aorta in a “V-shape” configuration [42]. Both vessels point to the left of the trachea (central and anterior to the spine), and the superior vena cava is located to the right of the aortic arch, and anterior to the trachea [42]. Yet, for the case herein, the 3VT view shows a “Y-shape” configuration, in which the aorta is anterior to the pulmonary artery (Figure 1 and Videoclip S1).

The four-chamber view diagnostic plane demonstrated dextrocardia, a dilated left ventricle, enlarged mitral valve with redundancy in leaflet tissue, severely hypoplastic right ventricle, tricuspid atresia caused by a thick membrane, enlarged right atrium, and large interatrial communication (widely patent foramen ovale vs. atrial septal defect) (Figure 1 and Videoclip S1). The morphological left ventricle was identified by its fine apical trabeculations and smooth septal surface. By activating VIS-Assistance®, a VSD was demonstrated, and it is evident that the severely hypoplastic right ventricle is truly hypoplastic (i.e. not hypoplastic due to an azimuth issue) [36,37]. Pulmonary veins were difficult to visualize and therefore, it was unclear which atrium they were entering. The five-chamber view diagnostic plane showed findings similar to that of the four-chamber view, as well as the VSD. Through VIS-Assistance®, the proximal portion of the superior vena cava is seen entering the right atrium, and the severely hypoplastic right ventricle remains small in size.

In the left ventricular outflow tract diagnostic plane/VIS-Assistance®, both ventricles can be seen, with the well-developed pulmonary artery arising from the left ventricle (Figure 1 and Videoclip S1). The diagnostic plane of the short-axis view of great vessels/right ventricular outflow tract appears abnormal. VIS-Assistance® shows the pulmonary artery arising from

the left ventricle, inferior vena cava entering the right atrium, Eustachian valve, and a hepatic vein.

In the abdomen/stomach view diagnostic plane/VIS-Assistance®, viscero-atrial situs solitus was determined by the location of the inferior vena cava (anterior and right of the spine), descending aorta (posterior and left of the spine), hepatic venous drainage, right-sided liver, and stomach on the left side (Videoclip S2). The VIS-Assistance® videoclip shows the inferior vena cava as well as the hepatic vein entering the right atrium on the right side. Moreover, the videoclip also shows dextrocardia, a dilated left ventricle, enlarged mitral valve with redundancy in leaflet tissue, severely hypoplastic right ventricle, tricuspid atresia caused by a thick membrane, enlarged right atrium, large interatrial communication (widely patent foramen ovale vs. atrial septal defect), and VSD (Videoclip S2). Because of the targeted automatic navigational movements in the abdomen/stomach view VIS-Assistance®, the 3VT itself (with the findings described previously) is also included in the videoclip. There was no evidence of the “double vessel” sign (dilated azygos vein and aorta), which is diagnostic of interrupted inferior vena cava with azygos continuation [43]. For the ductal arch view, the diagnostic plane appears abnormal. VIS-Assistance® shows what appears to be the “ductal arch”; however, the pulmonary artery is arising from the left ventricle. The inferior vena cava and hepatic vein enter the right atrium, and the Eustachian valve is visible.

In the aortic arch diagnostic plane, the aortic arch was initially not apparent. However, we took advantage of the technology which underpins FINE, and implemented a technique (called *triple VIS-Assistance®*) that is reported here for the first time to obtain the aortic arch. Triple VIS-Assistance® works in the following manner. For a given original diagnostic plane (e.g. DP original), after VIS-Assistance® is activated and a new echocardiography plane is obtained (DP new 1), one may replace the original diagnostic plane with this new plane so that it appears in the template of nine echocardiography views. This is accomplished by pressing a button titled “Update Diagnostic Plane” on the ultrasound machine. If VIS-Assistance® is activated again for “DP new 1”, and a new plane (DP new 2) is chosen to replace DP new 1, this is known as *double VIS-Assistance®.* When activating VIS-Assistance® a third time so that a new plane (DP new 3) replaces DP new 2 in the template of nine echocardiography views, this action is known as *triple VIS-Assistance®.* By implementing such a technique, the ascending aorta was identified arising from the hypoplastic right ventricle, and narrowing in the transverse aortic arch and isthmus region is apparent, consistent with coarctation of the aorta (Figure 1 and Videoclip S1). Finally, the venae cavae diagnostic plane/VIS-Assistance® shows the superior and inferior vena cava entering the right atrium. The same view also shows tricuspid atresia, and both ventricles.

It is noteworthy that automatic labeling was correct for all the echocardiography views except for three: 1) five chamber; 2) short-axis view of great vessels/right ventricular outflow tract; and 3) ductal arch. Thus, in summary FINE showed dextrocardia, situs solitus, tricuspid atresia, hypoplastic right ventricle, dilated left ventricle with enlarged mitral valve, enlarged right atrium, D-transposition of the great vessels, coarctation of the aorta, ventricular septal defect, and large interatrial communication. The pulmonary veins were difficult to visualize.

Delivery and Postnatal course

Serial ultrasound examinations were performed for fetal growth restriction, in which the estimated fetal weight and amniotic fluid volume were calculated, and evaluation of the biophysical profile score, and fetal Doppler velocimetry. At 37 weeks of gestation, the estimated fetal weight was 1877 grams (<5th percentile), the abdominal circumference lagged by 7 weeks, and there was oligohydramnios. The patient was sent to the hospital for evaluation, and non-stress testing was non-reactive. The next day, a repeat cesarean section and bilateral tubal ligation was performed. A uterine didelphys was identified with the fetus located in the right horn. The male neonate weighed 1690 grams, Apgar scores were 6 and 7 (1 and 5 minutes, respectively), and the umbilical cord arterial pH was 6.997.

After birth, the complex cardiac defect was confirmed by transthoracic echocardiography (Figure 2 and Videoclip S3) and cardiac catheterization. In addition, leftward juxtaposition of the atrial appendages was noted. Pulmonary venous return was normal into the left atrium. A moderate-sized atrial septal defect was identified in the secundum portion of the atrial septum, along with a large redundant fossa ovalis aneurysm. There were no extracardiac anomalies noted. Dextrocardia and a left-sided stomach bubble were also apparent on the chest x-ray (Figure 3). A diagram that conceptually depicts the congenital heart defect postnatally is shown in Figure 4.

The infant had a prolonged and complicated postnatal course and remained in the hospital until eight months of age. Due to his low birth weight, he underwent an initial “hybrid procedure” at two weeks of life, characterized by ductal stenting and bilateral pulmonary artery band placement, in order to establish secure systemic outflow and a controlled source of pulmonary blood flow (Figures 5 and 6, Videoclip S4). At 5 months of age, a Norwood reconstruction of the aortic arch with Sano modification was performed to proceed with single-ventricle palliation. The infant experienced multiple complications throughout the hospital course, including hypoxemia, pericardial effusions, infections, thromboses, and stroke, requiring multiple interventions and extracorporeal membrane oxygenation (ECMO) support. The patient was eventually discharged home, but was readmitted two months later with sepsis, disseminated intravascular coagulation, and multi-organ failure. Despite all efforts, he expired during that hospitalization.

Discussion

Intelligent navigation technology and characteristics of FINE

We report herein the first case of fetal dextrocardia with situs solitus and complex congenital heart disease successfully diagnosed using the FINE method. Situs solitus refers to the normal arrangement of organs and vessels within the body. Specifically, atrio-visceral situs solitus is characterized by the right inferior vena cava and superior vena cava connecting to the systemic right atrium on the right side of the heart, with a right-sided liver and left-sided stomach [44]. In the current case, although the cardiac axis from base to apex was directed rightward, and the fetal heart was located in the right side of the chest, there was still successful generation of nine fetal echocardiography views using a combination of diagnostic planes and/or VIS-Assistance®. This is possible because of the intelligent

navigation technology which underpins FINE [37]. Marking anatomical structures in different planes of the heart using intelligent navigation allows inferences of the anatomical relationships in multiple dimensions and therefore, geometrical reconstruction of the fetal heart is possible [36]. Indeed, a unique characteristic of FINE is that the method is *adaptive* (i.e. "fits" the anatomy of each particular case under examination) [36,37], similar to a professional tailor who makes unique modifications to the garment based upon a client's body shape and posture. Specifically, the successful display of cardiac diagnostic planes occurs in the presence of anatomic variability (e.g. cardiac axis and geometry) [36]. Moreover, all seven fetal anatomical structures which are marked using Anatomic Box® are cardiac structures and not that of the chest. Therefore, even with positional changes of the fetal heart (e.g. dextrocardia), the FINE method is still applicable and successful.

Manual navigation of a volume dataset by the operator is the traditional method of examining anatomical areas of interest in multiple sectional planes [37]. Yet, this requires operating the x, y, z controls, scaling, and parallel shifting. As a result, the retrieval and display of relevant diagnostic planes is often time-consuming, challenging, and tedious. Moreover, interrogating STIC volume datasets requires substantial knowledge of anatomy, considerable expertise, and tools used for interrogation (i.e. software) [37]. In contrast, intelligent navigation interrogates STIC volume datasets, and then automatically extracts and displays the diagnostic planes.

The "virtual" sonographer tool VIS-Assistance® was invaluable in this case of congenital heart disease because it delineated the complex anatomical relationships very well, which had been difficult to do in real-time sonography (Videoclip S2). This allowed us to make a more confident diagnosis and was also helpful in education and teaching. In addition, VIS-Assistance® provided information (e.g. coarctation of the aorta) that was not evident in the diagnostic plane [36] (Figure 1 and Videoclip S1). When compared to manual navigation within a STIC volume dataset by the sonologist, VIS-Assistance® has several unique characteristics and advantages [37]: 1) *automatic* navigation through the volume dataset; 2) *consistent* navigational movements through the volume each time that VIS-Assistance® is activated; 3) time duration of VIS-Assistance® is typically *shorter* (less than 4 minutes); and 4) the *types* of navigational movements through the volume are unique and would be difficult or impossible to perform otherwise.

We also found that the simultaneous display of multiple fetal echocardiography views (Figure 1 and Videoclip S1) was very useful and informative, since: 1) anatomical features of the complex cardiac defect could be visualized and compared side-by-side; and 2) the same abnormality could be confirmed in multiple views at the same time (e.g. hypoplasia of the transverse aortic arch) [36].

Automatic labeling through intelligent navigation of anatomical structures within the diagnostic planes is possible because the system "infers" the actual location of structures in space [37]. For the case herein, automatic labeling of anatomical structures was correct for six of the nine echocardiography views, and was correct in labeling all diagnostic planes, left and right sides of the fetus, and cranial and caudal ends. This is consistent with our expectations, since in cases of complex congenital heart disease, we have found that the

automatic labeling feature of the FINE method may not always be appropriate. It is noteworthy that despite the dextrocardia, labeling of the cardiac chambers in the four-chamber view diagnostic plane was accurate because our case was consistent with Type II dextrocardia (or *dextroversion*) as classified by Arcilla and Gasul (see below) [1].

When the FINE method was developed, we proposed using this as an aid for examination of the fetal heart in the population at large, rather than to diagnose specific congenital heart defects [36]. However, through further experience with such method, we have found that in cases of cardiac anomalies, FINE is able to demonstrate abnormal cardiac anatomy successfully [36]. Even in the setting of complex congenital heart disease, FINE can automatically generate informative fetal echocardiography views. In addition, we have recently reported that by combining color or bidirectional power Doppler with FINE (known as *5D Heart Color*), abnormal hemodynamic flow is demonstrated and the anatomic diagnosis is corroborated [39].

Dextrocardia and confusion in terminology

The position of the heart in the chest, and the orientation of the cardiac apex should be described separately, since these features can vary independently from each other, and have no definitive association with other cardiac relationships and connections [45]. Indeed, there is confusion in the literature and no general consensus as to the definition of *dextrocardia.* This term is most commonly understood to mean a heart lying predominantly in the right hemithorax [46]. Others describe dextrocardia as both cardiac placement on the anatomic right side, and a cardiac apex that points to the anatomic right [47]. Many authors use the definition of primary dextrocardia, a cardiac malposition in which the major axis of the heart (from base to apex along the interventricular septum) points to the right, and is due to an intrinsic developmental abnormality [1–5]. It is noteworthy, however, that in this context, dextrocardia only describe the position of the cardiac axis, and does not convey information about chamber organization and cardiac anatomy [2–4,7–10].

In 1961, Arcilla and Gasul evaluated the clinical, angiographic, and autopsy results on 50 patients with congenital dextrocardia, and classified this into 5 major types: 1) Type I (mirror-image dextrocardia); 2) Type II (dextroversion complex); 3) Type III (mixed dextrocardia); 4) Type IV (congenital dextroposition); and 5) Type V (congenital extrinsic) [1]. In such classification, Types 1 through IV represent the intrinsic group of dextrocardia, since this is caused by a developmental anomaly of the primitive heart tube. In contrast, for Type V dextrocardia the abnormal cardiac position is due to displacement by congenital anomalies of the lungs, diaphragm, or chest cage [1]. Based upon the classification system of Arcilla and Gasul, the case reported herein is consistent with Type II dextrocardia (i.e. relationship of the cardiac chambers are normal; the right atrium and right ventricle are situated to the right of, and posterior to the corresponding systemic chambers). Essentially, Type II dextrocardia is a simple rotation or pivoting of the heart to the right along the horizontal plane, with the atria as a fulcrum [7,48]. In a 1968 morphologic study of 41 cases of dextrocardia, Lev et al. identified 5 such cases of dextroversion, in which all of them were associated with situs solitus, which is also consistent with our findings [7].

Wilkinson and Acerete, as well as others, have noted that even more complicated definitions or additional terms about dextrocardia have been reported, and do not believe these are desirable since such terms are not universally understood and may be confusing (i.e. secondary dextrocardia, extrinsic dextrocardia, mixed dextrocardia, isolated dextrocardia, pivotal dextrocardia, dextroversion, dextrorotation, and dextroposition) [7,45,46]. Recently, Edwards and Maleszewski have recommended that a descriptive process should be implemented, to include the location of the heart and cardiac axis direction, so that specific terms can be avoided [49]. Moreover, a separate description of the location of the heart and direction of the cardiac apex is not just an academic exercise, but is important because it can profoundly affect planned surgical interventions [45] and precise communication is necessary.

Prenatal diagnosis of dextrocardia and association with congenital heart defects and situs type

It is known that in patients with situs solitus and dextrocardia, up to 96% will have abnormal intracardiac anatomy [3,44]. In a study of 125 patients (mean age 9.2 years) with dextrocardia who underwent echocardiography at a tertiary care center, 34.4% (n=43) had situs solitus dextrocardia [3]. Of this specific group, 39.5% (n=17) had discordant arterial connections, and only 7% (n=3) had normal intracardiac anatomy [3]. A retrospective chart review of dextrocardia at a tertiary care hospital in Canada identified a total of 81 cases, of which 48 were diagnosed prenatally, and 33 were diagnosed postnatally [44]. Of all the cases with situs solitus and dextrocardia (n=27), cardiac malformations were present in 96% (n=26), and they were often complex [44].

When fetal dextrocardia is identified, a comprehensive assessment of fetal cardiac anatomy should be performed, since this is associated with multiple and complex congenital cardiac anomalies [3]. Specifically, careful attention should be given to determining the situs of abdominal organs, relationship of atria to ventricles, great vessel location, and venous drainage. Moreover, complex cardiac malformations are more frequent in the setting of dextrocardia with situs solitus and situs ambiguous, than with situs inversus [2–5,9,10]. Indeed, Table 1 shows that in cases of fetal dextrocardia with situs solitus diagnosed on prenatal ultrasound, the frequency of congenital heart disease ranges from 50% to 100% [2,4–6,44,48,50].

In several studies of prenatally diagnosed dextrocardia, situs solitus was the most frequent type of situs (46-60%) (Table 1) [2,4,50]. Bernasconi et al. studied 81 fetuses with dextrocardia diagnosed at two tertiary care centers of fetal cardiology [2]. In this population, situs solitus was the most common (47%; n=38) type of situs, and 66% (25/38) of these cases had structural cardiac malformations. Similarly, a recent study reported the incidence of situs solitus to be 46% in cases of primary dextrocardia diagnosed prenatally [4]. Of such cases, the frequency of cardiac defects was 80% (8/10). In contrast, Walmsley et al. reported that situs solitus was the least frequent situs type (22%); however, 100% of the ten fetuses with dextrocardia and situs solitus had a cardiac malformation (Table 1) [5].

Tricuspid Atresia

Tricuspid atresia is a cyanotic cardiac defect with congenital absence or agenesis of the tricuspid valve, occurring in 0.08 per 1,000 live births [51]. During prenatal screening, the incidence is 1/15,000, or 0.47% of all cardiac defects detected [52]. In this condition, the right atrium is hypertrophied and dilated, there is an interatrial communication (e.g. atrial septal defect or patent foramen ovale), and the right ventricle is hypoplastic. The mitral valve has a large orifice, and the left ventricle is dilated with wall hypertrophy. A ventricular septal defect is almost always present, typically in the inlet septum. The vessel which arises from the small right ventricle tends to be hypoplastic. Thus, in the setting of concordant ventriculoarterial connection, pulmonary stenosis or atresia is frequently found, especially when the ventricular septal defect is small, and the aorta is either normal, or slightly larger than normal [53]. However, in cases of ventriculoarterial discordance (found in the case herein), hypoplasia of the aortic arch, coarctation, or even aortic atresia may occur, depending upon the size of the ventricular septal defect [53,54]. This is because in the setting of tricuspid atresia and D-transposition of the great vessels, an increased portion of blood flows into the pulmonary artery and through the ductus arteriosus into the descending aorta. As a result, flow through the aorta and aortic arch is decreased.

In tricuspid atresia, the relationship of the great vessels varies, and is the basis for classification types: 1) type I: normally related great vessels (70-80% of cases); 2) type II: D-transposition of the great vessels (12-25% of cases); 3) type III: great vessel positional abnormalities other than D-transposition of the great vessels (e.g. L-transposition of the great vessels) and 4) type IV: persistent truncus arteriosus [55–57]. The case reported herein is consistent with type II tricuspid atresia.

Juxtaposition of the atrial appendages is an associated defect of tricuspid atresia [58,59], and was noted in our case postnatally (juxtaposition to the left side). This is a rare condition in which both appendages, or one and part of the other, lie adjacent on one side of the great arterial pedicle [60]. In almost every case, this occurs in the setting of complex congenital heart disease, and its presence usually indicates severe cyanotic heart disease [60,61]. Left juxtaposition, in which both atrial appendages lie to the left of the great vessels, is more common than right juxtaposition. The incidence of left juxtaposed atrial appendages in tricuspid atresia has been reported to be about 10% [59].

The combination of tricuspid atresia and dextrocardia is extremely rare [62]. Van Praagh et al. reviewed 136 patients with dextrocardia in an autopsy series [63]. Tricuspid atresia was found in only a single patient, and situs solitus with L-transposition of the great vessels was identified. In contrast, our fetus was affected with D-transposition of the great vessels.

Tricuspid atresia or abnormalities in the tricuspid valve combined with situs solitus and dextrocardia have been reported in a handful of reports [3,7,44,53,62,64,65]. In 1968, Lev et al. conducted a morphologic study of 41 cases of dextrocardia [7]. One male neonate at 4 days of life had the following findings, which were almost identical to the current case: situs solitus, dextrocardia, tricuspid atresia, complete transposition of the great vessels, ventricular septal defect, coarctation of the aorta, aneurysm of the fossa ovalis, and

juxtaposition of the atrial appendages. In addition, a patent ductus arteriosus, and double left atrium were identified [7].

In a 1980 case report, the authors described a 13 year old boy with situs solitus, dextrocardia, tricuspid atresia, D-transposition of the great vessels and subaortic conus, atrial septal defect, and massive mitral valve insufficiency with dilated left atrium [62]. At 8 months of age, he had undergone a pulmonary artery banding procedure. Upon presentation, a right atrial to pulmonary artery conduit procedure and mitral valve replacement successfully repaired the child's circulation and he was completely asymptomatic 1 year after the surgery [62]. This case is very similar to ours, but with a different post-operative outcome.

Two recent large studies have reported the postnatal outcomes when tricuspid atresia has been diagnosed prenatally [53,66]. In a multicenter study conducted at three tertiary care institutions, the authors identified 88 fetuses with tricuspid atresia and found an 83% survival at 1 year for liveborn infants, with no subsequent deaths for 13 years [66]. Through multivariate analysis, two independent factors were significantly associated with an increase in time-related mortality in those that were actively managed: 1) presence of a chromosomal anomaly or syndrome (hazard ratio (HR) 13.3; 95% confidence interval (CI) 2.21-19.6); and 2) the need for ECMO (HR 11.3; 95% CI 2.26-56.2) [66]. While our fetus did not have a chromosomal anomaly or additional extracardiac defects, ECMO stabilization was required postnatally, and is likely a surrogate for increased morbidity. Another study of 54 cases of tricuspid atresia found that the short-term overall survival in continuing pregnancies was 89.2%, with the greatest loss rate occurring in the first year postnatally [53]. However, there was an increase in the mortality rate in subsequent years [67].

Conclusion

Fetal dextrocardia is usually associated with a wide spectrum of cardiac defects that are complex. We report for the first time, a case of fetal dextrocardia and situs solitus with complex congenital heart disease in which Fetal Intelligent Navigation Echocardiography (FINE) was invaluable in diagnosing the multiple cardiac defects and defining the complex anatomic relationships. Until now, such technology has never been applied to cases of fetal cardiac malposition.

Supplementary Material

Refer to Web version on PubMed Central for supplementary material.

Acknowledgments

An application for a patent ("Apparatus and Method for Fetal Intelligent Navigation Echocardiography") has been filed with the U.S. Patent and Trademark Office and the patent is pending. Dr. Lami Yeo and Dr. Roberto Romero are co-inventors, along with Mr. Gustavo Abella and Mr. Ricardo Gayoso. The rights of Dr. Yeo and Dr. Romero have been assigned to Wayne State University, and NICHD/NIH, respectively. None of the authors has a financial relationship with either Samsung Healthcare, Seoul, Korea, or Medge Platforms, Inc., New York, NY, USA.

The work of Dr. Romero was supported by the Perinatology Research Branch, Division of Intramural Research, *Eunice Kennedy Shriver* National Institute of Child Health and Human Development, NIH, DHHS. Dr. Romero has

contributed to this work as part of his official duties as employee of the United States Federal Government. Dr. Lami Yeo was funded by Wayne State University through a service contract in support of the Perinatology Research Branch.

This research was supported, in part, by the Perinatology Research Branch, Division of Intramural Research, *Eunice Kennedy Shriver* National Institute of Child Health and Human Development, National Institutes of Health, Department of Health and Human Services (NICHD/NIH/DHHS); and, in part, with Federal funds from NICHD, NIH under Contract No. HHSN275201300006C.

References

1. Arcilla RA, Gasul BM. Congenital dextrocardia. Clinical, angiocardiographic, and autopsy studies on 50 patients. J Pediatr. 1961; 58:39–58. [PubMed: 13684051]
2. Bernasconi A, Azancot A, Simpson JM, Jones A, Sharland GK. Fetal dextrocardia: diagnosis and outcome in two tertiary centres. Heart. 2005; 91:1590–1594. [PubMed: 16287744]
3. Garg N, Agarwal BL, Modi N, Radhakrishnan S, Sinha N. Dextrocardia: an analysis of cardiac structures in 125 patients. Int J Cardiol. 2003; 88:143–155. [PubMed: 12714192]
4. Oztunc F, Madazli R, Yuksel MA, Gökalp S, Oncul M. Diagnosis and outcome of pregnancies with prenatally diagnosed fetal dextrocardia. J Matern Fetal Neonatal Med. 2015; 28:1104–1107. [PubMed: 25007986]
5. Walmsley R, Hishitani T, Sandor GG, Lim K, Duncan W, Tessier F, Farquharson DF, Potts JE. Diagnosis and outcome of dextrocardia diagnosed in the fetus. Am J Cardiol. 2004; 94:141–143. [PubMed: 15219529]
6. Falkensammer CB, Ayres NA, Altman CA, Ge S, Bezold LI, Eidem BW, Kovalchin JP. Fetal cardiac malposition: incidence and outcome of associated cardiac and extracardiac malformations. Am J Perinatol. 2008; 25:277–281. [PubMed: 18401841]
7. Lev M, Liberthson RR, Eckner FA, Arcilla RA. Pathologic anatomy of dextrocardia and its clinical implications. Circulation. 1968; 37:979–999. [PubMed: 5653057]
8. Calcaterra G, Anderson RH, Lau KC, Shinebourne EA. Dextrocardia - value of segmental analysis in its categorisation. Br Heart J. 1979; 42:497–507. [PubMed: 518773]
9. Huhta JC, Hagler DJ, Seward JB, Tajik AJ, Julsrud PR, Ritter DG. Two-dimensional echocardiographic assessment of dextrocardia: a segmental approach. Am J Cardiol. 1982; 50:1351–1360. [PubMed: 7148713]
10. Stanger P, Rudolph AM, Edwards JE. Cardiac malpositions. An overview based on study of sixty-five necropsy specimens. Circulation. 1977; 56:159–172. [PubMed: 872306]
11. Evans WN, Acherman RJ, Collazos JC, Castillo WJ, Rollins RC, Kip KT, Restrepo H. Dextrocardia: practical clinical points and comments on terminology. Pediatr Cardiol. 2010; 31:1–6. [PubMed: 19727926]
12. Veronese P, Bogana G, Cerutti A, Yeo L, Romero R, Gervasi MT. A prospective study of the use of Fetal Intelligent Navigation Echocardiography (FINE) to obtain standard fetal echocardiography views. Fetal Diagn Ther. 2017; 41:89–99. [PubMed: 27309391]
13. DeVore GR, Falkensammer P, Sklansky MS, Platt LD. Spatiotemporal image correlation (STIC): new technology for evaluation of the fetal heart. Ultrasound Obstet Gynecol. 2003; 22:380–387. [PubMed: 14528474]
14. Goncalves LF, Lee W, Chaiworapongsa T, Espinoza J, Schoen ML, Falkensammer P, Treadwell M, Romero R. Four-dimensional ultrasonography of the fetal heart with spatiotemporal image correlation. Am J Obstet Gynecol. 2003; 189:1792–1802. [PubMed: 14710117]
15. Chaoui R, Hoffmann J, Heling KS. Three-dimensional (3D) and 4D color Doppler fetal echocardiography using spatio-temporal image correlation (STIC). Ultrasound Obstet Gynecol. 2004; 23:535–545. [PubMed: 15170792]
16. Yagel S, Cohen SM, Shapiro I, Valsky DV. 3D and 4D ultrasound in fetal cardiac scanning: a new look at the fetal heart. Ultrasound Obstet Gynecol. 2007; 29:81–95. [PubMed: 17200988]
17. Rizzo G, Capponi A, Muscatello A, Cavicchioni O, Vendola M, Arduini D. Examination of the fetal heart by four-dimensional ultrasound with spatiotemporal image correlation during routine

second-trimester examination: the ‘three-steps technique’. Fetal Diagn Ther. 2008; 24:126–131. [PubMed: 18648213]

18. Bennasar M, Martínez JM, Olivella A, del Río M, Gómez O, Figueras F, Puerto B, Gratacós E. Feasibility and accuracy of fetal echocardiography using four- dimensional spatiotemporal image correlation technology before 16 weeks’ gestation. Ultrasound Obstet Gynecol. 2009; 33:645–651. [PubMed: 19479815]
19. Yeo L, Romero R, Jodicke C, Ogge G, Lee W, Kusanovic JP, Vaisbuch E, Hassan S. Four-chamber view and ‘swing technique’ (FAST) echo: a novel and simple algorithm to visualize standard fetal echocardiographic planes. Ultrasound Obstet Gynecol. 2011; 37:423–431. [PubMed: 20878671]
20. Yeo L, Romero R, Jodicke C, Kim SK, Gonzalez JM, Ogge G, Lee W, Kusanovic JP, Vaisbuch E, Hassan S. Simple targeted arterial rendering (STAR) technique: a novel and simple method to visualize the fetal cardiac outflow tracts. Ultrasound Obstet Gynecol. 2011; 37:549–556. [PubMed: 20878672]
21. Luewan S, Yanase Y, Tongprasert F, Srisupundit K, Tongsong T. Fetal cardiac dimensions at 14-40 weeks’ gestation obtained using cardio-STIC-M. Ultrasound Obstet Gynecol. 2011; 37:416–422. [PubMed: 21305637]
22. Barros FS, Moron AF, Rolo LC, Rocha LA, Martins WP, Tonni G, Nardozza LM, Araujo Júnior E. Fetal myocardial wall area: constructing a reference range by means of spatiotemporal image correlation in the rendering mode. Fetal Diagn Ther. 2015; 37:44–50. [PubMed: 25095802]
23. Nardozza LM, Rolo LC, Araujo Júnior E, Hatanaka AR, Rocha LA, Simioni C, Ruano R, Moron AF. Reference range for fetal interventricular septum area by means of four-dimensional ultrasonography using spatiotemporal image correlation. Fetal Diagn Ther. 2013; 33:110–115. [PubMed: 23295684]
24. Viñals F. Current experience and prospect of internet consultation in fetal cardiac ultrasound. Fetal Diagn Ther. 2011; 30:83–87. [PubMed: 21849765]
25. Godfrey ME, Messing B, Valsky DV, Cohen SM, Yagel S. Fetal cardiac function: M- mode and 4D spatiotemporal image correlation. Fetal Diagn Ther. 2012; 32:17–21. [PubMed: 22777135]
26. Crispi F, Gratacós E. Fetal cardiac function: technical considerations and potential research and clinical applications. Fetal Diagn Ther. 2012; 32:47–64. [PubMed: 22614129]
27. Yeo L, Romero R. How to Acquire Cardiac Volumes for Sonographic Examination of the Fetal Heart: Part 1. J Ultrasound Med. 2016; 35:1021–1042. [PubMed: 27091914]
28. Yeo L, Romero R. How to Acquire Cardiac Volumes for Sonographic Examination of the Fetal Heart: Part 2. J Ultrasound Med. 2016; 35:1043–1066. [PubMed: 27091912]
29. Goncalves LF, Espinoza J, Romero R, Lee W, Beyer B, Treadwell MC, Humes R. A systematic approach to prenatal diagnosis of transposition of the great arteries using 4-dimensional ultrasonography with spatiotemporal image correlation. J Ultrasound Med. 2004; 23:1225–1231. [PubMed: 15328439]
30. Paladini D, Sglavo G, Greco E, Nappi C. Cardiac screening by STIC: can sonologists performing the 20-week anomaly scan pick up outflow tract abnormalities by scrolling the A-plane of STIC volumes? Ultrasound Obstet Gynecol. 2008; 32:865–870. [PubMed: 19035539]
31. Gindes L, Hegesh J, Weisz B, Gilboa Y, Achiron R. Three and four dimensional ultrasound: a novel method for evaluating fetal cardiac anomalies. Prenat Diagn. 2009; 29:645–653. [PubMed: 19340842]
32. Bennasar M, Martínez JM, Gómez O, Bartrons J, Olivella A, Puerto B, Gratacós E. Accuracy of four-dimensional spatiotemporal image correlation echocardiography in the prenatal diagnosis of congenital heart defects. Ultrasound Obstet Gynecol. 2010; 36:458–464. [PubMed: 20549767]
33. Espinoza J, Lee W, Comstock C, Romero R, Yeo L, Rizzo G, Paladini D, Viñals F, Achiron R, Gindes L, Abuhamad A, Sinkovskaya E, Russell E, Yagel S. Collaborative study on 4-dimensional echocardiography for the diagnosis of fetal heart defects: the COFEHD study. J Ultrasound Med. 2010; 29:1573–1580. [PubMed: 20966468]
34. Adriaanse BM, Tromp CH, Simpson JM, Van Mieghem T, Kist WJ, Kuik DJ, Oepkes D, Van Vugt JM, Haak MC. Interobserver agreement in detailed prenatal diagnosis of congenital heart disease by telemedicine using four-dimensional ultrasound with spatiotemporal image correlation. Ultrasound Obstet Gynecol. 2012; 39:203–209. [PubMed: 21611994]

35. Gómez O, Soveral I, Bennasar M, Crispi F, Masoller N, Marimon E, Bartrons J, Gratacós E, Martinez JM. Accuracy of fetal echocardiography in the differential diagnosis between truncus arteriosus and pulmonary atresia with ventricular septal defect. Fetal Diagn Ther. 2016; 39:90–99. [PubMed: 26113195]
36. Yeo L, Romero R. Fetal Intelligent Navigation Echocardiography (FINE): a novel method for rapid, simple, and automatic examination of the fetal heart. Ultrasound Obstet Gynecol. 2013; 42:268–284. [PubMed: 24000158]
37. Yeo L, Romero R. Intelligent navigation to improve obstetrical sonography. Ultrasound Obstet Gynecol. 2016; 47:403–409. [PubMed: 26525650]
38. Garcia M, Yeo L, Romero R, Haggerty D, Giardina I, Hassan SS, Chaiworapongsa T, Hernandez-Andrade E. Prospective evaluation of the fetal heart using Fetal Intelligent Navigation Echocardiography (FINE). Ultrasound Obstet Gynecol. 2016; 47:450–459. [PubMed: 26278116]
39. Yeo L, Romero R. Color and power Doppler combined with Fetal Intelligent Navigation Echocardiography (FINE) to evaluate the fetal heart. Ultrasound Obstet Gynecol. 2017; 50:476–491. [PubMed: 28809063]
40. Classification of overweight and obesity by BMI, waist circumference, and associated disease risks. https://www.nhlbi.nih.gov/health/educational/lose_wt/BMI/bmi_dis.htm
41. Ring LE. The anesthetic approach to operative delivery of the extremely obese parturient. Semin Perinatol. 2014; 38:341–348. [PubMed: 25146109]
42. Gardiner H, Chaoui R. The fetal three-vessel and tracheal view revisited. Semin Fetal Neonatal Med. 2013; 18:261–268. [PubMed: 23466189]
43. Sheley RC, Nyberg DA, Kapur R. Azygous continuation of the interrupted inferior vena cava: a clue to prenatal diagnosis of the cardiosplenic syndromes. J Ultrasound Med. 1995; 14:381–387. [PubMed: 7609017]
44. Bohun CM, Potts JE, Casey BM, Sandor GG. A population-based study of cardiac malformations and outcomes associated with dextrocardia. Am J Cardiol. 2007; 100:305–309. [PubMed: 17631088]
45. Jacobs JP, Anderson RH, Weinberg PM, Walters HL 3rd, Tchervenkov CI, Del Duca D, Franklin RC, Aiello VD, Béland MJ, Colan SD, Gaynor JW, Krogmann ON, Kurosawa H, Maruszewski B, Stellin G, Elliott MJ. The nomenclature, definition and classification of cardiac structures in the setting of heterotaxy. Cardiol Young. 2007; 17(Suppl 2):1–28.
46. Wilkinson JL, Acerete F. Terminological pitfalls in congenital heart disease. Reappraisal of some confusing terms, with an account of a simplified system of basic nomenclature. Br Heart J. 1973; 35:1166–1177. [PubMed: 4761119]
47. Lambert TE, Kuller J, Small M, Rhee E, Barker P. Abnormalities of fetal situs: an overview and literature review. Obstet Gynecol Surv. 2016; 71:33–38. [PubMed: 26819133]
48. Comstock CH, Smith R, Lee W, Kirk JS. Right fetal cardiac axis: clinical significance and associated findings. Obstet Gynecol. 1998; 91:495–499. [PubMed: 9540929]
49. Edwards WD, Maleszewski JJ. Cardiac anatomy and examination of cardiac specimens. In: Allen HD, Driscoll DJ, Shaddy RE, Feltes TF, editorsMoss and Adams' Heart Disease in Infants, Children, and Adolescents. Vol. 1. Williams & Wilkins; 2013. 1–31.
50. Ozkutlu S, Bostan OM, Deren O, Onderoğlu L, Kale G, Güçer S, Orhan D. Prenatal echocardiographic diagnosis of cardiac right/left axis and malpositions according to standardized Cordes technique. Anadolu Kardiyol Derg. 2011; 11:131–136. [PubMed: 21303758]
51. Hoffman JI, Kaplan S. The incidence of congenital heart disease. J Am Coll Cardiol. 2002; 39:1890–1900. [PubMed: 12084585]
52. Tegnander E, Williams W, Johansen OJ, Blaas HG, Eik-Nes SH. Prenatal detection of heart defects in a non-selected population of 30,149 fetuses - detection rates and outcome. Ultrasound Obstet Gynecol. 2006; 27:252–265. [PubMed: 16456842]
53. Berg C, Lachmann R, Kaiser C, Kozlowski P, Stressig R, Schneider M, Asfour B, Herberg U, Breuer J, Gembruch U, Geipel A. Prenatal diagnosis of tricuspid atresia: intrauterine course and outcome. Ultrasound Obstet Gynecol. 2010; 35:183–190. [PubMed: 20101636]

54. Tongsong T, Sittiwangkul R, Wanapirak C, Chanprapaph P. Prenatal diagnosis of isolated tricuspid valve atresia: report of 4 cases and review of the literature. J Ultrasound Med. 2004; 23:945–950. [PubMed: 15292563]
55. Tandon R, Edwards JE. Tricuspid atresia. A re-evaluation and classification. J Thorac Cardiovasc Surg. 1974; 67:530–542. [PubMed: 4818528]
56. Rao PS. A unified classification for tricuspid atresia. American Heart Journal. 1980; 99:799–804. [PubMed: 6990738]
57. Rao PS Tricuspid Atresia. Curr Treat Options Cardiovasc Med. 2000; 2:507–520. [PubMed: 11096554]
58. Nath MP, Makhija N, Kiran U, Dhawan N, Velayoudam D. Left juxtaposed atrial appendages in a patient with dextrocardia and tricuspid atresia: TEE images. Ann Card Anaesth. 2011; 14:150–151. [PubMed: 21636938]
59. Thoele DG, Ursell PC, Ho SY, Smith A, Bowman FO, Gersony WM, Anderson RH. Atrial morphologic features in tricuspid atresia. J Thorac Cardiovasc Surg. 1991; 102:606–610. [PubMed: 1833594]
60. Abdullah M, Yoo SJ, Lee YH, Smallhorn J, Hornberger LK. Diagnosis of left juxtaposition of the atrial appendages in the fetus. Cardiol Young. 2000; 10:220–224. [PubMed: 10824902]
61. Van Praagh S, O'Sullivan J, Brili S, Van Praagh R. Juxtaposition of the morphologically left atrial appendage in solitus and inversus atria: a study of 18 postmortem cases. Am Heart J. 1996; 132(2 Pt 1):391–402. [PubMed: 8701903]
62. Jennings RB Jr, Crisler C, Johnson DH, Brickman RD. Tricuspid atresia with dextrotransposition, dextrocardia, and mitral insufficiency: successful circulatory correction. Ann Thorac Surg. 1980; 29:369–372. [PubMed: 7362331]
63. Van Praagh R, Weinberg PM, Van Praagh S. Malposition of the heart. In: Moss AJ, Adams FH, Emmanouilides GC, editorsHeart Disease in Infants, Children, and Adolescents. Williams & Wilkins; 1977. 394
64. Campbell M, Deuchar DC. Dextrocardia and isolated laevocardia. II Situs inversus and isolated dextrocardia. Br Heart J. 1966; 28:472–487. [PubMed: 5942468]
65. Shaher RM, Johnson AM. Isolated laevocardia and isolated dextrocardia. Pathology and pathogenesis. Guys Hosp Rep. 1963; 112:127–151. [PubMed: 13988366]
66. Wald RM, Tham EB, McCrindle BW, Goff DA, McAuliffe FM, Golding F, Jaeggi ET, Hornberger LK, Tworetzky W, Nield L. Outcome after prenatal diagnosis of tricuspid atresia: a multicenter experience. Am Heart J. 2007; 153:772–778. [PubMed: 17452152]
67. Sittiwangkul R, Azakie A, Van Arsdell GS, Williams WG, McCrindle BW. Outcomes of tricuspid atresia in the Fontan era. Ann Thorac Surg. 2004; 77:889–894. [PubMed: 14992893]

Established Facts

- Fetal dextrocardia is usually associated with a wide spectrum of cardiac defects that are often complex, making this condition conceptually difficult to understand and diagnose.
- Four-dimensional sonography with spatiotemporal image correlation (STIC) can facilitate examination of the fetal heart; however, analyzing STIC volume datasets is operator dependent and can be very challenging, especially when the heart is abnormal.
- A novel method known as Fetal Intelligent Navigation Echocardiography (FINE) automatically generates and displays nine standard fetal echocardiography views in normal hearts by applying intelligent navigation technology to STIC volume datasets.

Novel Insights

- The FINE method may be applied successfully to fetal dextrocardia with complex congenital heart disease, and demonstrates both abnormal fetal cardiac anatomy and complex anatomic relationships.

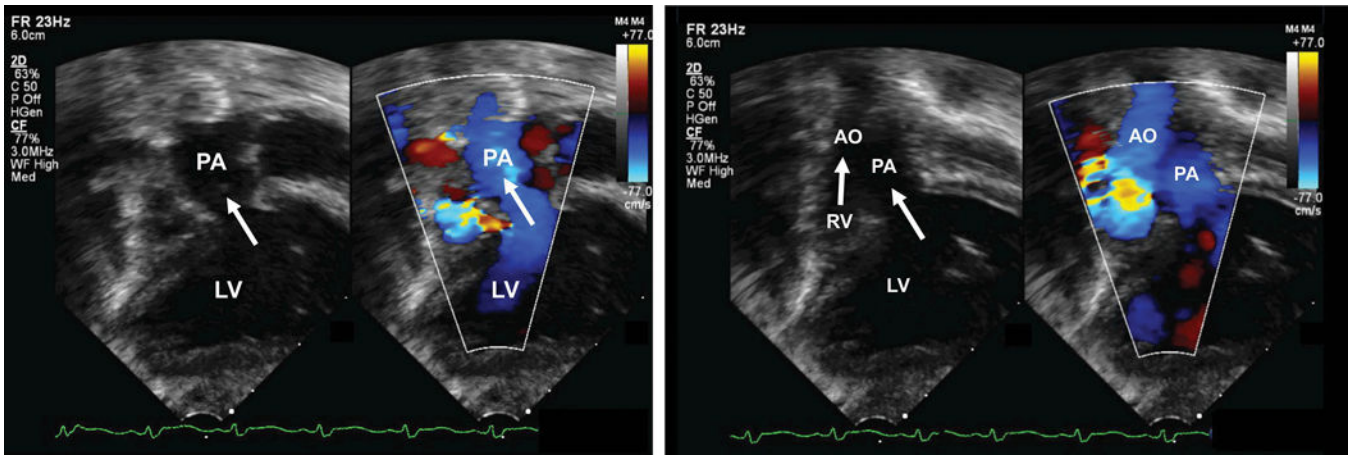

Figure 1.

Application of the Fetal Intelligent Navigation Echocardiography (FINE) method to a spatiotemporal image correlation (STIC) volume dataset of a fetus with dextrocardia, situs solitus, and complex congenital heart disease at 35 weeks of gestation (Videoclip S1). Nine cardiac diagnostic planes are displayed automatically in a single template with automatic labeling of the fetal left and right sides, cranial and caudal direction, each diagnostic plane, and anatomical structures. All of the nine echocardiography views are abnormal [diagnostic planes and/or Virtual Intelligent Sonographer Assistance (VIS-Assistance®)]. The three-vessels and trachea view diagnostic plane shows the well-developed leftward pulmonary artery arising from the dilated left ventricle, while a hypoplastic aorta is rightward and anterior to the pulmonary artery, and arises from the hypoplastic right ventricle (ventricle not shown in this frame) (i.e. D-transposition of the great vessels). Note that the three-vessel and trachea view shows a “Y-shape” configuration, in which the aorta is anterior to the pulmonary artery. In addition, automatic labeling by FINE is correct. The four-chamber view diagnostic plane shows dextrocardia, a dilated left ventricle, enlarged mitral valve with redundancy in leaflet tissue, severely hypoplastic right ventricle, tricuspid atresia caused by a thick membrane, enlarged right atrium, and large interatrial communication. Note that automatic labeling of all four chambers by FINE is correct. The five-chamber view diagnostic plane shows findings similar to that of the four-chamber view, as well as a ventricular septal defect. The “Ao” label here does not actually point to the aorta itself; however, the label is precisely where the aorta should exit from the hypoplastic right ventricle. In the left ventricular outflow tract diagnostic plane, the well-developed pulmonary artery arises from the left ventricle (not well shown in this frame). For the short-axis view of great vessels/right ventricular outflow tract, VIS-Assistance® was activated to show this plane, which appears abnormal. The pulmonary artery arises from the dilated left ventricle (the “RV” automatic label is incorrect here). In the abdomen view diagnostic plane, viscero-atrial situs solitus was determined by the location of the inferior vena cava (anterior and right of the spine), descending aorta (posterior and left of the spine), hepatic venous drainage (not shown here), right-sided liver, and stomach on the left side. For the ductal arch view, VIS-Assistance® was activated to show this image, which appears abnormal. The pulmonary artery arises from the dilated left ventricle (the “RV” automatic label is incorrect here). For the aortic arch view, *triple VIS-Assistance®* was performed to obtain the plane

displayed here. The ascending aorta is seen arising from the hypoplastic right ventricle, and narrowing in the transverse aortic arch and isthmus region is consistent with coarctation of the aorta. Note that automatic labeling of the aortic arch view by FINE is correct. The venae cavae diagnostic plane shows the superior and inferior vena cava entering the right atrium. In the superior part of the image, tricuspid atresia (between the right atrium and ventricle), is shown. A, transverse aortic arch; Ao, aorta; Desc., descending; IVC, inferior vena cava; LA, left atrium; LV, left ventricle; P, pulmonary artery; PA, pulmonary artery; RA, right atrium; RV, right ventricle; RVOT, right ventricular outflow tract; S, superior vena cava; SVC, superior vena cava; Trans., transverse

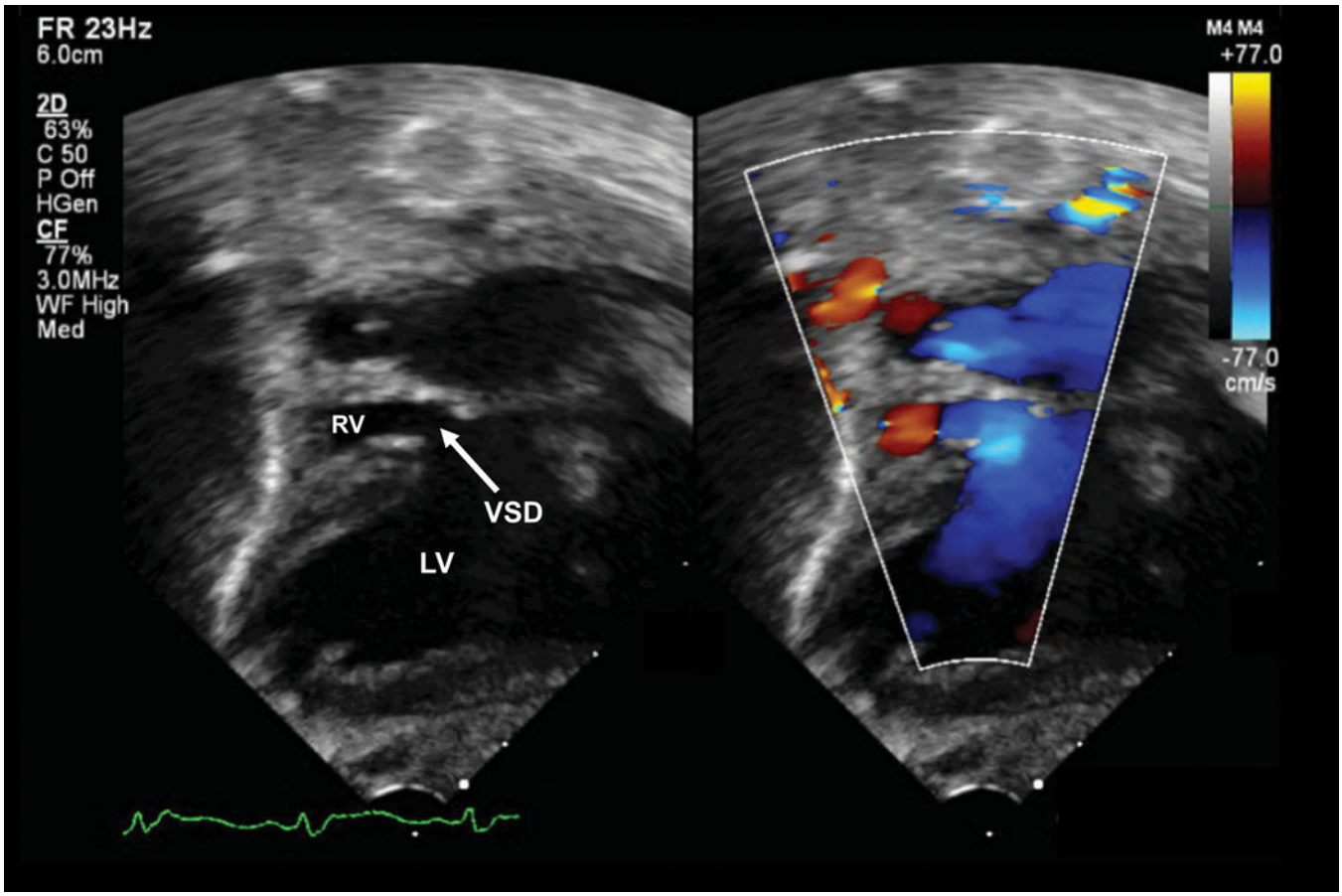

Figure 2.

Postnatal echocardiogram of the subcostal four-chamber view at day one of life (Videoclip S3). Dextrocardia is evident (cardiac axis from base to apex pointing to the neonatal right side), along with a dilated left ventricle and hypoplastic right ventricle. There is a thick membrane between the right atrium and ventricle where the tricuspid valve should be, but no true connection (tricuspid atresia). There is redundant atrial septal tissue bowing from right to left into the left atrium and a moderate-sized atrial septal defect in the secundum portion of the atrial septum. The ventricular septal defect is not seen in this imaging plane. LA, left atrium; LV, left ventricle; RA, right atrium; RV, right ventricle.

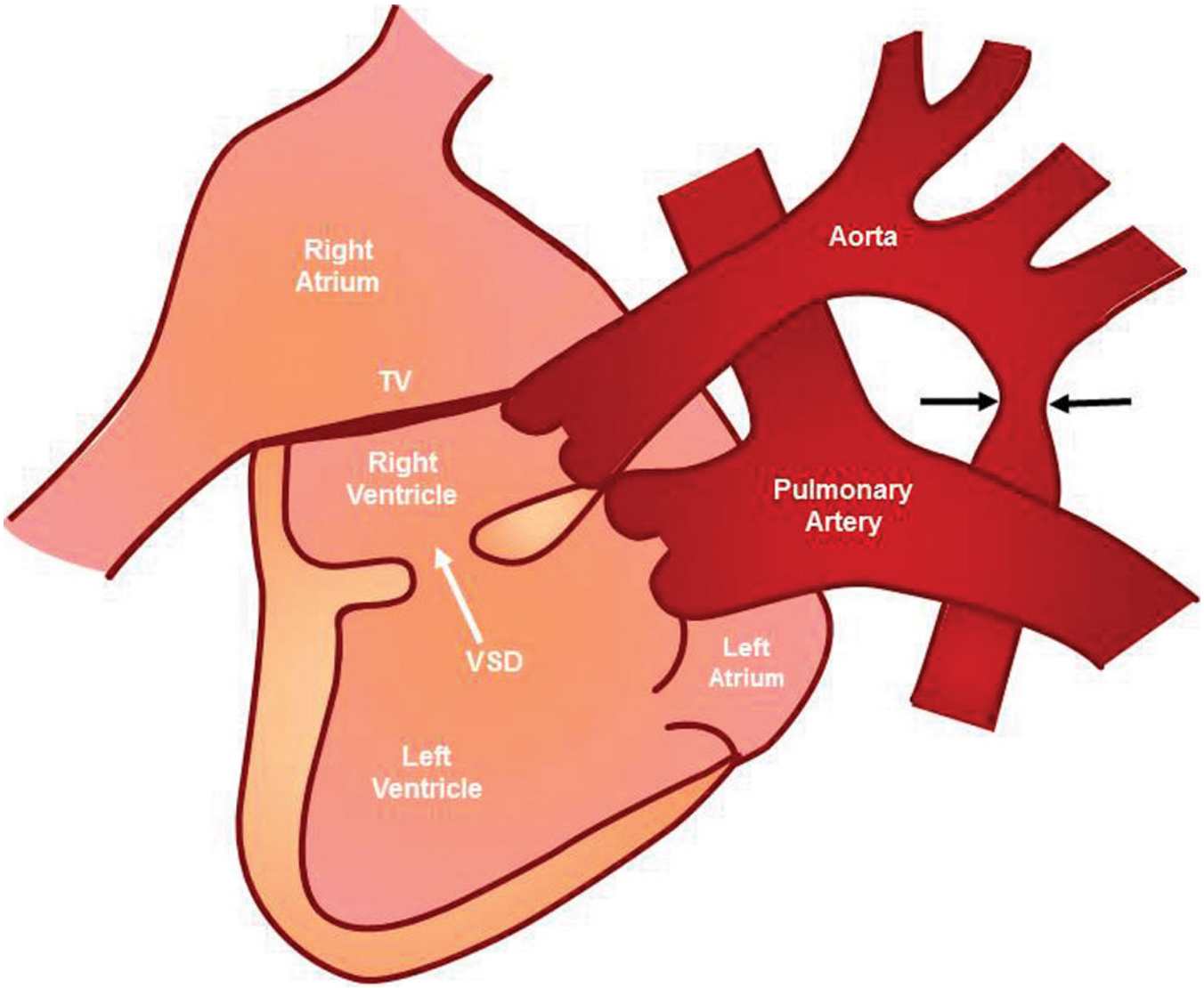

Figure 3.

Chest radiograph in the neonate shows dextrocardia, with discordant location of the cardiac apex (right-sided) relative to the stomach (left-sided). The feeding tube (thin, white line) is seen coursing leftward into the stomach bubble. The liver is located on the right side. R, neonatal right side.

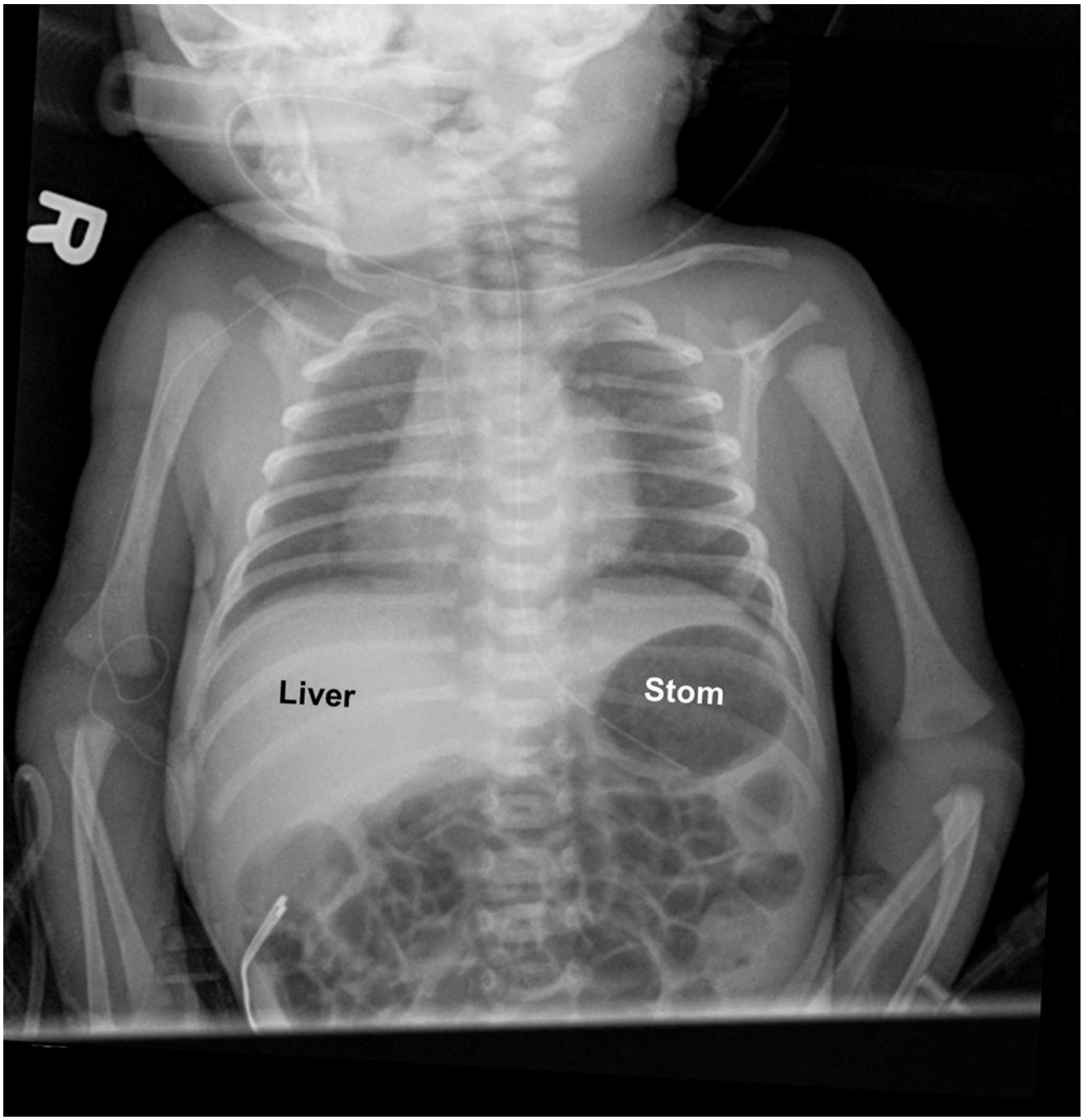

Figure 4.

Postnatal diagram of the current case (for conceptual purposes only). The left side of the diagram corresponds with the neonatal right side. There is dextrocardia, tricuspid atresia (thick membrane in red), hypoplastic right ventricle, enlarged right atrium, dilated left ventricle, D-transposition of the great vessels (well-developed leftward pulmonary artery arises from the left-sided morphologic left ventricle, while a hypoplastic aorta is rightward and anterior to the pulmonary artery, arising from the right-sided morphologic right

ventricle), coarctation of the aorta (black arrows point to narrowing of the isthmus), and ventricular septal defect (VSD) (white arrow). TV, tricuspid valve.

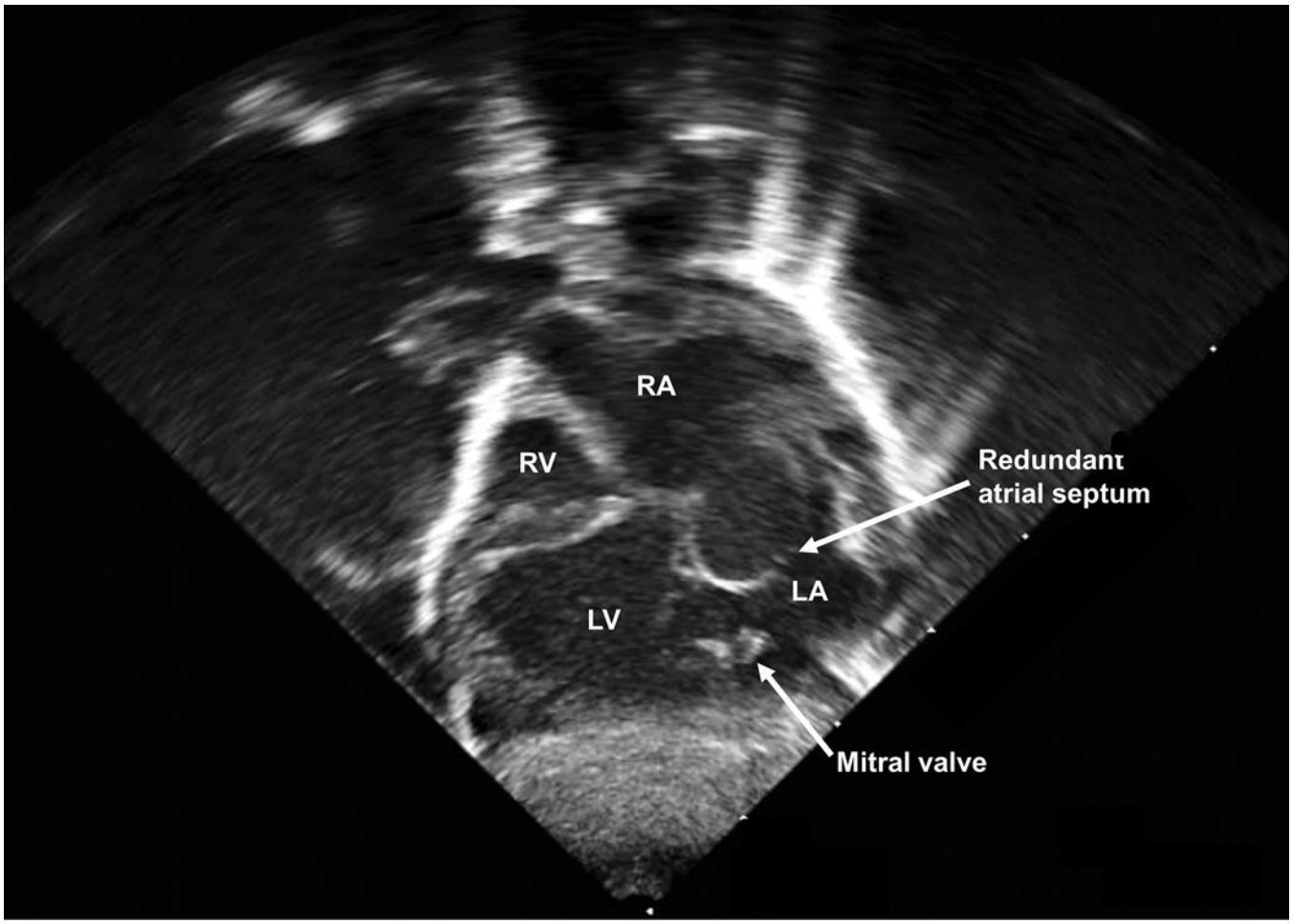

Figure 5.

Pediatric echocardiogram performed at 2 weeks of life after hybrid procedure showing the subcostal four-chamber view (Videoclip S4). Left, gray scale; Right, color Doppler. Dextrocardia is evident (cardiac axis from base to apex pointing to the neonatal right side), along with a dilated left ventricle and hypoplastic right ventricle. There is a membrane between the right atrium and ventricle, but with no true connection (tricuspid atresia). Color flow is demonstrated from the left to right ventricle through the small, restrictive ventricular septal defect. More superiorly in the image, a stent (circular, white echogenic structure) is visualized in the main pulmonary artery from the previous hybrid procedure. (Note that the color Doppler bar orientation does not correspond to the color Doppler flow depicted in the heart, because the image has been flipped for illustrative purposes). LV, left ventricle; RV, right ventricle; VSD, ventricular septal defect.

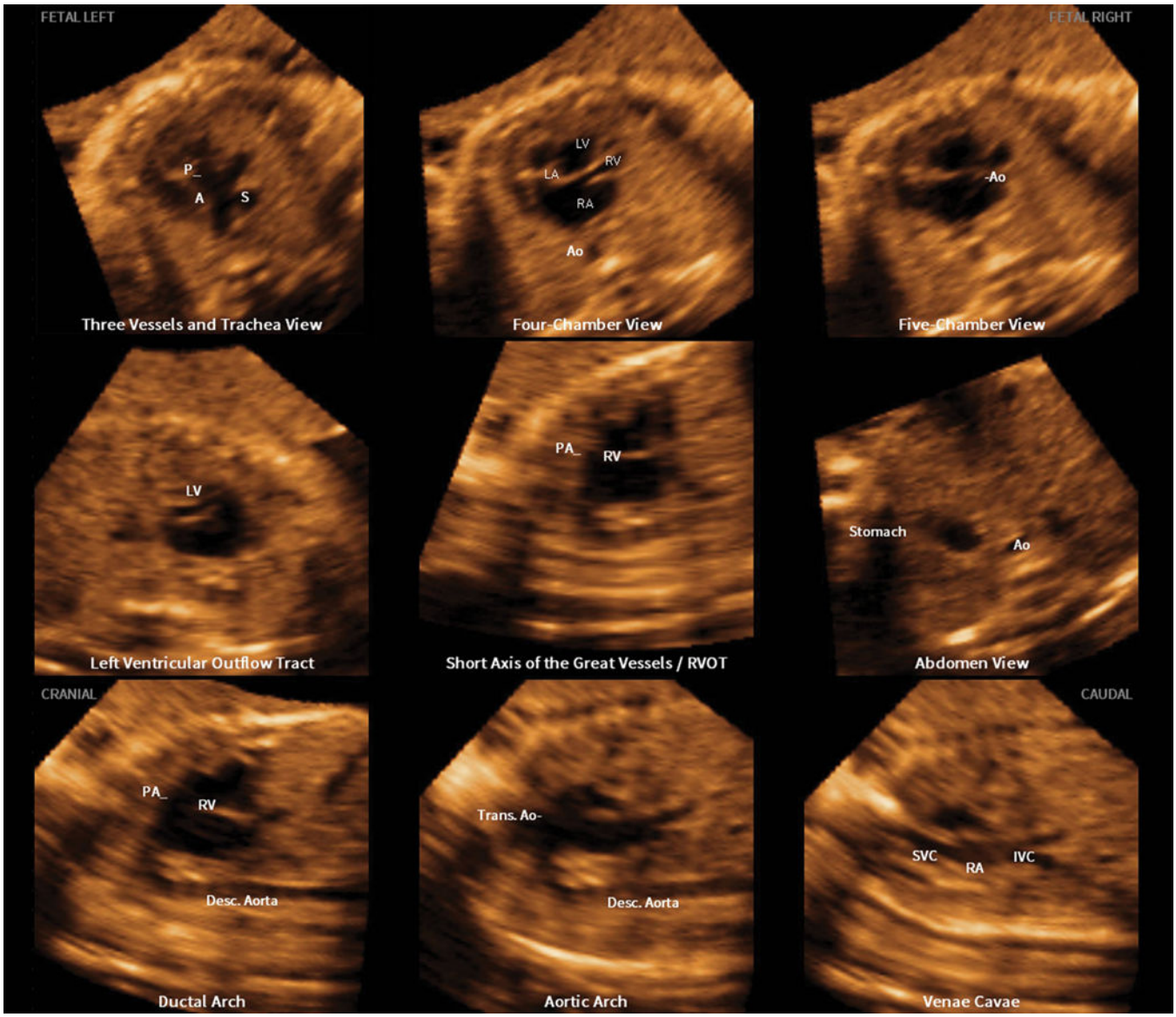

Figure 6.

Pediatric echocardiogram performed at 2 weeks of life after hybrid procedure showing the great vessels exiting the ventricles (Videoclip S4). Dextrocardia is evident (cardiac axis from base to apex pointing to the neonatal right side), along with a dilated left ventricle and hypoplastic right ventricle. A) The pulmonary artery is seen exiting from the left ventricle (blue color), and the initial portion of the pulmonary artery bifurcation is seen on the gray scale image. At the top of the image, a stent (circular, white echogenic structure) is visualized in the main pulmonary artery from the previous hybrid procedure. B) From the right ventricle, there is flow (blue color) through the aorta, which is smaller, rightward, and anterior to the larger pulmonary artery. (Note that the color Doppler bar orientation does not correspond to the color Doppler flow depicted in the heart, because the image has been

flipped for illustrative purposes). AO, aorta; LV, left ventricle; PA, pulmonary artery; RV, right ventricle.

Table 1

Cases of fetal dextrocardia and situs solitus diagnosed on prenatal ultrasound

First author, year [Ref.]	Dextrocardia cases (n)	Definition of dextrocardia	Situs type % (n)			Frequency of CHD with situs solitus and dextrocardia % (n)
			SS	SI	SA	
Comstock (1998) [48]	22	- Defined as a right cardiac axis[a] - Any fetus with abnormal heart position was not included	N/A	N/A	N/A	68% (15) of all dextrocardia cases had CHD (frequency for situs solitus alone unavailable)
Walmsley (2004) [5]	46	- Right-sided position of the heart (most of the heart located in the right hemithorax) - Direction of apex was not a criteria	22% (10)	39% (18)	39% (18)	100% (10)
Bernasconi (2005) [2]	81	- Major axis of the heart points to the right - Fetuses with dextroposition (heart shifted into the right chest due to an extracardiac abnormality) were excluded	47% (38)	23% (19)	30% (24)	66% (25)
Bohun (2007) [44]	81 total cases - 48 diagnosed prenatally - 33 diagnosed postnatally	- Right-sided embryologic development of the heart with most of the heart mass positioned in the right hemithorax	33%[b] (27)	37%[b] (30)	30%[b] (24)	For all cases of situs solitus (diagnosed both pre- and postnatally), CHD was found in 96% (26/27)
Falkensammer (2008) [6]	26	- Fetal heart positioned in the right chest, with the apex pointing to the right	23% (6)	8% (2)	69% (18)	50% (3)
Ozkutlu (2011) [50]	10	- Heart located in the right hemithorax with the apex pointing to the right	60% (6)	30% (3)	10% (1)	100% (6)
Oztunc (2015) [4]	22	- Right-sided positioning of the heart (most of the heart in the right hemithorax) - Direction of apex was not a criterion - Primary dextrocardia (due to embryologic development)	46% (10)	18% (4)	36% (8)	80% (8)

CHD, congenital heart disease; N/A, not available; SA, situs ambiguous; SI, situs inversus; SS, situs solitus.

[a]Cardiac axes from 25 degrees to the left of midline to anywhere in the midline or right chest.

[b]No information on situs types for prenatally diagnosed cases only.